Supplementary Information of Boreal Env. Res. Vol. 30: 55–76, 2025

Supplementary Information of

Environmental magnetism assessing coastal deoxygenation history in the northern Baltic Sea during Holocene thermal maximum from a high time resolution sedimentary sequence

***Silvennoinen et al*.**

Correspondence to: Sonja Silvennoinen (sonja.silvennoinen@helsinki.fi)

S1. Sediment sampling intervals

Details on sampling of sediment core KY15 for lithological and environmental magnetic measurements presented in Table S1 and S2 respectively. Below, detailed explanation on each method is given. For environmental magnetic methods, a short explanation on each parameter is given.

Table S1. Methods used in the study and measurement interval.

Property	Method	Number of subsamples / measurements	Interval
Magnetic susceptibility	Surface scan	363 / 646	10 cm / 1 cm*
Organic content	Loss on ignition	109	50 cm & contacts
Grain size	Laser diffraction	60	50 cm / 1 m** & contacts
Macro fossil for dating	AMS radiocarbon	3	-
Bulk sediment for dating	AMS radiocarbon	4	-
Environmental magnetic characteristics	See Table S2	23	5–50 cm, selected depths, units 2–4

* 10 cm interval from the whole core and 1cm interval from four depths (6.8–8 m, 15–17 m, 19–21.8 m and 27–28 m)

** 50 cm interval on sections where environmental magnetic characteristics were measured, otherwise 1 m interval and where grain size variations were observed during logging

.: Environmental magnetic measurements

method	equipment and used settings	demagnetization / acquisition steps
NRM & demag.	2G-SQUID magnetometer	0, 2.5, 5, 7.5, 10, 15, 20, 30, 40, 60, 80, 100, + 120, 140, 160 mT
from freeze dried subsamples:		
RRM acquisition	Molspin triple mu-metal shielded AF demagnetizer, 50 Hz, AF 100 mT, 5 rps	AF 100 mT in +Z-direction, 100 mT in -Z-direction. Demagnetizing as in NRM. Prior static demagnetization in +Z-direction.
ARM acquisition	LDA3 demagnetizer+ AMU-1A	100 mT peak AF and 0.1 mT bias field along +Z-axis. Demagnetizing as in NRM.
IRM acquisition, S-ratio	Pulse magnetizer MMPM 10	3000 mT in +Z-directions and 100 mT along -z axis. Demagnetizing as in NRM.
Frequency dependent susceptibility	SM105, Field 320 A/m, frequency 1: 512 Hz, frequency 2: 8000 Hz	

NRM – natural remanent magnetization
RRM – rotational remanent magnetization
ARM – anhysteretic remanent magnetization
IRM – isothermal remanent magnetization

S2. Grain size determination

The grain size distribution was analysed using laser diffraction method. Prior to analysis, the subsamples were diluted in a small amount of distilled water and treated to dissolve organic matter, diatoms and carbonates. To remove organic matter, subsamples were heated with 5 ml of 30 % H_2O_2, adding more of the peroxide until chemical reaction seized completely and excess peroxide could be boiled from the subsample with water. To remove diatoms, approx. 80 ml of 10 % NaOH was added and brought to a boil for 5 minutes. Lastly to remove carbonates, 5 ml of 10 % HCl was added and brought to a boil for 60 seconds. Beakers were filled with distilled water and left to settle for at least overnight and decanted when clear. For subsamples from depths 0.8–9.7 m NaOH treatment was not applied, and for subsamples from depths 10.7–15.7 m NaOH treatment was done last after carbonate removal. Before the analysis, 0.0134 M sodium pyrophosphate ($Na_4P_2O_7$) was added as a dispersant and subsamples were treated with ultrasonic vibration for 60 seconds to avoid flocculation. Grain size distributions were analysed with a Malvern Mastersizer 2000 Laser Diffractometer with an analytical range of ~0.02–2000 μm and an error of < 2%, (30 s measurement time, 15 s in between of measurements, pump speed 2100 RPM, stirrer speed 550 RPM) as a 5-measurement-average. Sediment with d50-value below 2 μm is defined as clay and d50-value between 2–60 μm is defined as silt. However, due to the underestimation of the clay percentage by laser diffraction method (Konert and Vandenberghe 1997), 6.3 μm if used to represent the 2μm clay boundary (Ramaswamy and Rao 2006). When organic content of the sediment exceeds 2%, the sediment is defined as gyttja clay/silt, as defined by the Geological Survey of Finland (Haavisto-Hyvärinen and Kutvonen 2007).

S3. Water depth, relative shoreline displacement estimation and age-depth model

Past water depth of the study site shown in Figures 2 and 6 was estimated based on the relative shoreline displacement curve (Figure S1) and tentative age-depth model (Figure S2) for the KY15 sediment core. Shore displacement curve was compiled from dated isolation observation from this study (radiocarbon date from depth 0.61 m), nearby isolation and landform observations from the Ancient Shoreline Database (Geological Survey of Finland), Eronen (1974), Glückert *et al.* (1993) and Vuorela *et al.* (2009). Landform observations (n=14) were 2–76 km away from the study site, and isolation observations (n=6) 64–123 km away. Sites that were near the same isostatic uplift isobase as Kurikka were preferred, and elevation was corrected for sites away from the isobase to correspond the uplift in Kurikka using figure 17 in Glückert *et al.* (1993). The tentative age-depth model was constructed using the Bacon software (Blaauw and Christen 2011) (Figure S2). Uncalibrated accepted radiocarbon dates and the estimated deglaciation time was used as inputs. Bacon calibrated the dates using IntCal 20-curve and basic programme settings were used.

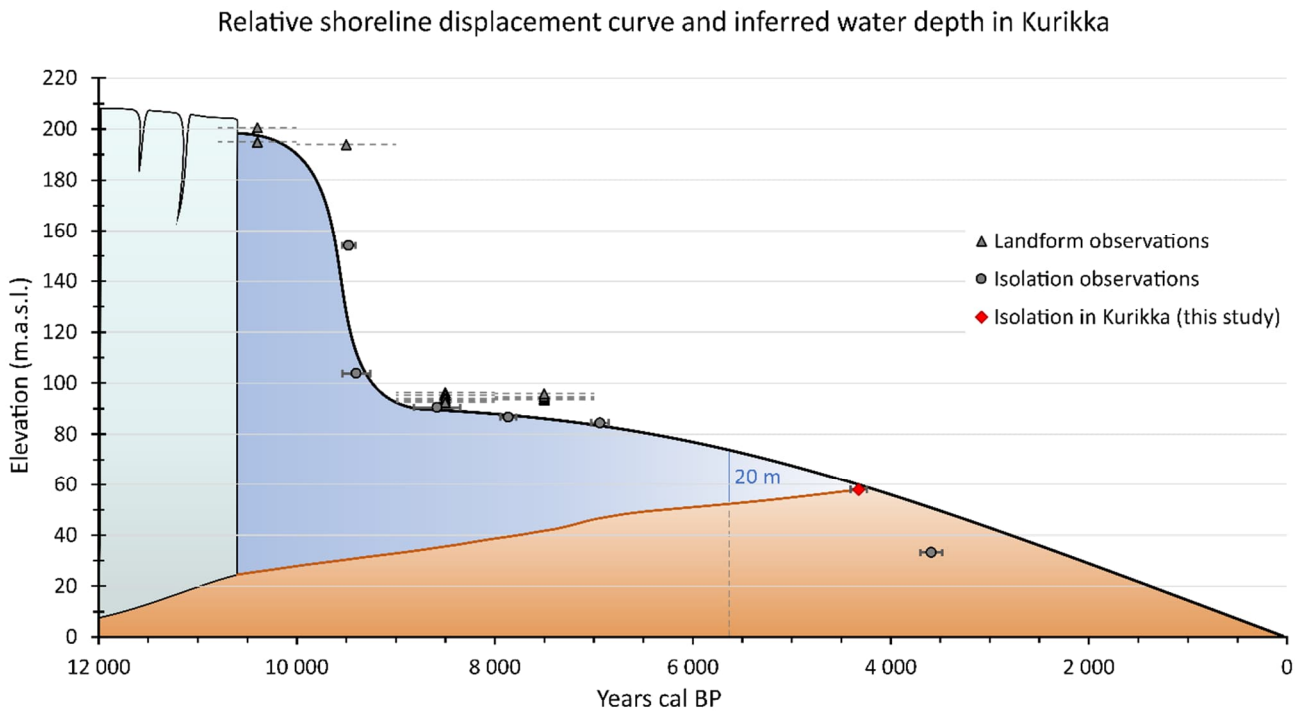

Figure S1. Relative shoreline distribution curve for Kurikka, Southern Ostrobothnia. Depth of sediment during deposition (brown) estimated based on the tentative age-depth model. Estimated water depth at the study site shown in blue. Deglaciation (ice depicted as light turquoise) time (10.6 ka) according to Stroeven *et al.* (2016).

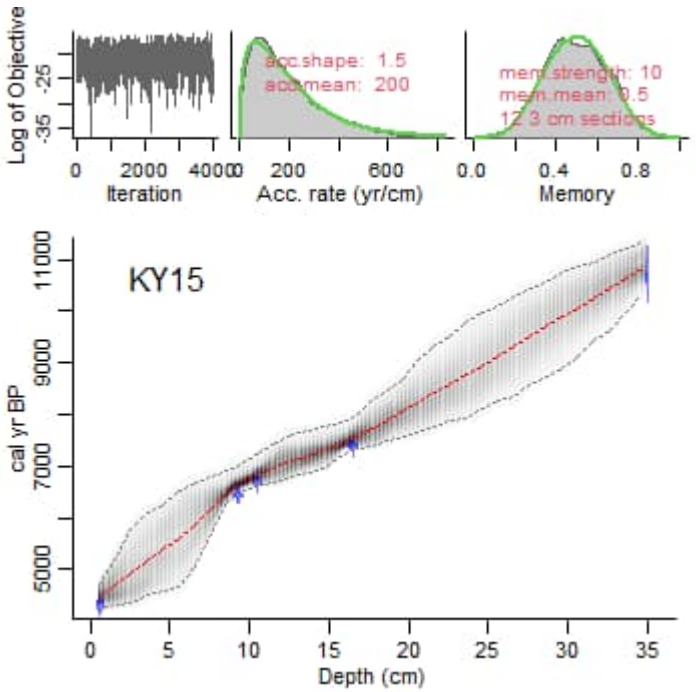

Figure S2. Tentative age-depth model for KY15 constructed in the Bacon software. Estimated deglaciation time for Kurikka was used as the basal age for the model. Other age points are based on radiocarbon dating (see results ch. 4.1. and Table 1).

S4. Environmental magnetic methods

The environmental magnetic methods aim to measure concentration of magnetic minerals, identify these minerals and determine their grain size. Magnetic susceptibility (κ), natural remanent magnetization (NRM), anhysteretic remanent magnetization (ARM), and saturation isothermal remanent magnetization (SIRM) are concentration dependent parameters. Most of these parameters primarily reflect changes in ferrimagnetic mineral concentrations because ferrimagnetic materials (such as greigite, (Ti-)magnetite and maghemite) have the highest intrinsic magnetization of all known natural materials (Hunt *et al.* 1995). Magnetic susceptibility reflects the combined magnetic response of all ferromagnetic, paramagnetic, and diamagnetic materials, whereas SIRM is affected by only ferromagnetic minerals. This includes contributions from both low-coercivity ('soft', ferrimagnetic) magnetic grains that are easier to magnetize and demagnetize and high-coercivity minerals ('hard', antiferromagnetic) that require stronger magnetic fields to become magnetized. ARM captures only the contribution of low-coercivity minerals grains in the sample, such as greigite and magnetite. To estimate the relative amount of high- and low-coercivity remanence in a sample, S-ratio ($IRM_{-0.1T}/IRM_{3T}$) is calculated (Stober and Thompson 1979, Reinholdsson *et al.* 2013). S-ratio is close to -1 when ferrimagnetic low coercivity minerals such as magnetite and greigite dominate.

Both mineralogy and grain size affect magnetic coercivity. Coercivity can be expressed with the median destructive field of demagnetization curves (MDF_{NRM}), i.e. the field that is needed to halve the natural remanent magnetization in a sample (e.g. Maher 2011, Liu *et al.* 2012) For the relatively low-coercivity mineral magnetite, the MDF_{NRM} is, depending on grain size, ~15–30 mT (Dankers 1981, Dunlop 1986), the coercivity of greigite being slightly higher (Roberts 1995). However, due to grain size variations, their signals can also overlap. Usually, higher MDF values suggest smaller average grain sizes (Maher 2011). In addition to MDF, SD greigite is known for the acquisition of a significant rotational remanent magnetization (RRM) (Snowball 1997). Stephenson (1980) explained it in terms of a gyroremanent effect associated with a flip of magnetic moments during AF demagnetization. The magnitude of RRM is diagnostically considerably higher for greigite compared to magnetite (Snowball 1997). RRM is imparted on samples after static demagnetizing by simultaneously rotating and demagnetizing the sample, and after this measuring the produced magnetization. The RRM is expressed in relation to the rotation vector (see Figure S3), where parallel magnetization produces a positive RRM (Stephenson and Snowball 2001) and with antiparallel magnetization, the sign of RRM is negative. This is done in both sample +z and -z -directions, and the average of the measurements is calculated.

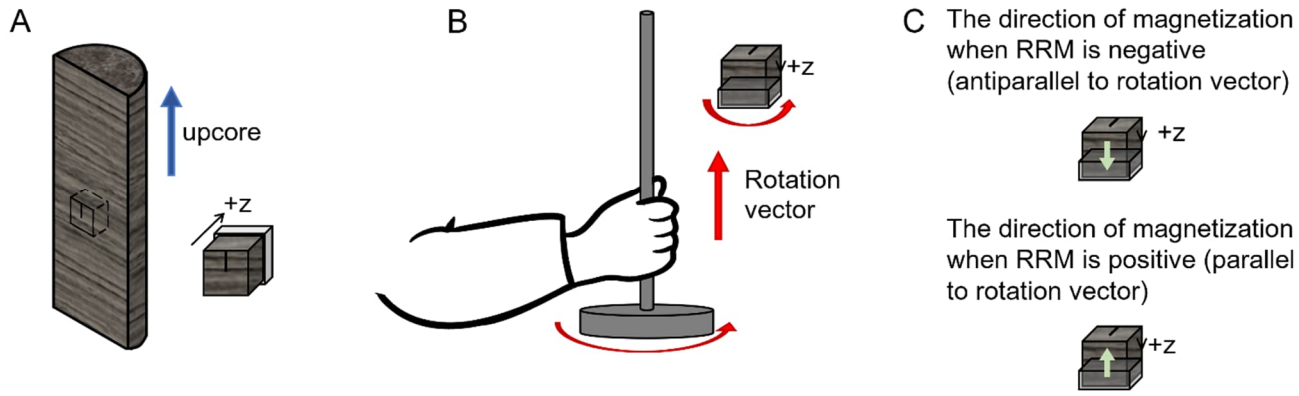

Figure S3. A: Subsampling method and subsample coordinates in relation to core and sediment structure. Sediment core is unoriented. B: RRM is expressed in relation to the rotation vector, where the right-hand rule is applied. C: When acquired magnetization is parallel to the rotation vector, the RRM sign is positive, and when the acquired magnetization is antiparallel to the rotation vector, the RRM sign is negative. Arrow colours: Black: Subsample coordinate; Blue: Up core direction; Red: rotation vector direction; Green: Acquired magnetization direction.

Because the magnitude of RRM is proportional to the abundance of the magnetic minerals in the sample, RRM can be normalized by the biasing (direct) field imposed during ARM acquisition (Potter and Stephenson 1986). The resulting effective gyro field (Bg = b x (RRM/ARM); b = biasing field, 100 uT) can be used alongside RRM to distinguish the carriers of RRM. Of all other magnetic minerals, greigite has the highest known effective gyrofield (several hundred μT for a peak AF of 80 mT; Snowball (1997)), making Bg a good indicator of greigite.

Thermomagnetic analyses can also be used to investigate magnetic mineralogy of powdered samples. Magnetic minerals become paramagnetic and lose magnetic susceptibility when heated to specific temperatures (Curie or Néel temperatures). The Curie temperatures for stoichiometric magnetite and monoclinic pyrrhotite are 580C and 325C, respectively (Dekkers 1989, Dunlop and Özdemir 1997). The Néel temperature for stoichiometric hematite is 675°C (Dunlop and Özdemir 1997). Although the Curie temperature for greigite is not known (e.g., Roberts 1995, Dekkers *et al.* 2000, Roberts *et al.* 2011), greigite exhibits some diagnostic behaviour when heated (Dekkers *et al.* 2000, Muxworthy *et al.* 2023). Magnetic susceptibility of greigite drops between ~250°C and ~400°C during heating (e.g., Snowball and Thompson 1988, Roberts 1995, Dekkers *et al.* 2000, Roberts *et al.* 2011), due to its transformation into sulphur, pyrite, marcasite, and pyrrhotite (Skinner *et al.* 1964, Krs *et al.* 1992, Dekkers *et al.* 2000). Depending on the amount of oxygen present when heated, either hematite (abundant air), magnetite (restricted air) or pyrrhotite and magnetite (air excluded) is produced in samples containing greigite (Dekkers *et al.* 2000). In addition, some magnetic minerals display crystallographic changes in cryogenic temperatures that aid in their identification, such as stoichiometric magnetite, which shows the Verwey transition at around 120 K (Verwey 1939).

The magnetic properties of magnetic minerals are dependent on grain size. Very small magnetic particles behave superparamagnetically (SP), mid-sized grains have a single magnetic domain (SD), and big grains feature multiple domains (MD). SD-grains are magnetically stable and have the highest coercive force, while MD-grains are usually magnetically softer. The absolute grain sizes for these classes depend on the mineral. For greigite, threshold for SP behaviour is estimated as 0.03–0.05 μm, SD behaviour has been observed with natural grains spreading 0.03–0.115 μm and grains above 0.5–0.7 μm should start showing MD behaviour (Roberts *et al.* 2011). Magnetosomal (produced by magnetotactic bacteria) SD grains have usually a narrower size distribution than authigenic minerals,

this type of greigite is on average ~0.07 μm. Presence of SP ferrimagnetic grains can be detected by measuring magnetic susceptibility with two different frequencies (i.e., frequency dependent susceptibility, $\chi_{fd} = 100\times\chi_{lf}-\chi_{hx}/\chi_{lx}$), where larger χ_{fd} values suggest a larger amount of SP grains. According to Dearing (1999), 2–10% χ_{fd} in natural environmental samples indicate a mixture of SP grains, and the theoretical maximum credible χ_{fd} percentage is 14 %. In addition to this, ARM can be used to distinguish relative ferrimagnetic SD and MD contributions. High ARM correlates strongly with SD-grains (Potter and Stephenson 1986, Maher 1988), whereas MD and SP-grains do not acquire ARM. Since ARM is proportional to the field used to generate it, ARM is normalized with this field to produce comparable values across laboratories (Evans and Heller 2003). The produced value is called as the susceptibility of ARM ($\chi_{ARM} = ARM/H_{dc}$, H_{dc} = 79.58 A/m with 100 mT bias field). Due to SIRM being fairly insensitive to different sizes (Evans and Heller 2003) and χ_{ARM} being strongly size dependent, the relative abundance of SD magnetite grains can be estimated by the ratio of χ_{ARM}/SIRM (King *et al.* 1982, Maher 2011), with higher values indicating higher SD fraction. Totally concentration independent parameter χ_{ARM}/χ ratio is used to study relative contributions of SP and SD grains to the bulk signal (e.g., Banerjee *et al.* 1981, Evans and Heller 2003). The χ_{ARM} is strongly size dependent whereas low field magnetic susceptibility χ shows same value over a very wide range of grain sizes. Very small SP and large multi-domain (MD) grains carry higher magnetic susceptibility, but lower ARM than SD grains. Especially, SP grains are supposed not to carry remanence (Maher 1988). Therefore, for SD grains the value of this ratio is high and for MD and SP grain the value is lower (e.g., King *et al.* 1982).

S5. Imaging and elemental analysis

Carbon-coated, magnetically extracted grains from subsample 15.75 were imaged using a JEOL JXA-iSP100 electron microprobe at 15 kV, operated in backscattered electron compositional mode (BED-C) at HelLabs, University of Helsinki. Energy dispersive spectroscopy (EDS) with a silicon drift detector (SDD) was used to analyze the grains, and Fe/S ratios were calculated to determine mineralogy. Both greigite and pyrite aggregates/framboids were identified, with greigite composed of smaller grains than pyrite (Fig. S4). The grain size of greigite was below the detection limit of the instrument. The Fe/S ratios of 0.69–0.75 correspond to that of greigite (0.75), and while the ratios of 0.37–0.4 are lower than of pure pyrite (0.5), these ratios are interpreted to indicate pyrite grains. The offset between measured and expected ratios might derive from partial oxidation and interference with surrounding material, as the small size of the grains makes it probable that the measurement has focused on both the mineral grain and the surrounding matrix (Roberts *et al.* 2011, Chen *et al.* 2021, Ucar *et al.* 2024).

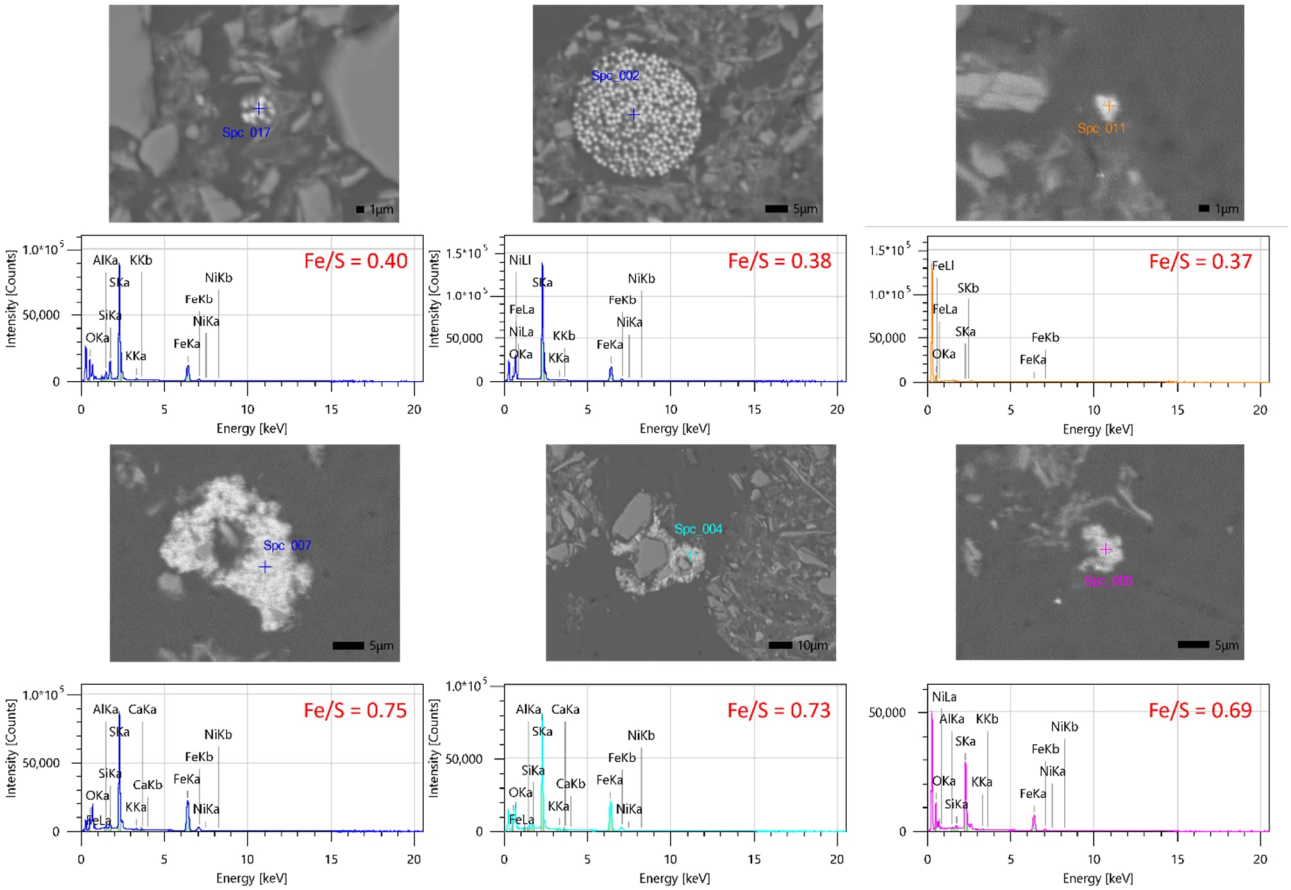

Figure S4. Images and elemental analysis of individual Fe-S grains and grain aggregates from the subsample 15.75. Fe/S ratios close to 0.4 are interpreted as pyrite, while ratios around 0.7 indicate greigite. The size of individual grains in greigite aggregates is below detection limit of the instrument.

S6. References

Banerjee S.K., King J. & Marvin J. 1981. A rapid method for magnetic granulometry with applications to environmental studies. *Geophysical Research Letters* 8: 333-336.

Blaauw M. & Christen J.A. 2011. Flexible paleoclimate age-depth models using an autoregressive gamma process. *Bayesian Analysis* 6: 457-474.

Chen Y., Zhang W., Nian X., Sun Q., Ge C., Hutchinson S.M., Cheng Q., Wang F., Chen J. & Zhao X. 2021. Greigite as an Indicator for Salinity and Sedimentation Rate Change: Evidence From the Yangtze River Delta, China. *Journal of Geophysical Research: Solid Earth* 126: e2020JB021085.

Dankers P. 1981. Relationship between median destructive field and remanent coercive forces for dispersed natural magnetite, titanomagnetite and hematite. *Geophysical Journal of the Royal Astronomical Society* 64: 447-461.

Dearing J.A. 1999. Environmental magnetic susceptibility using the Bartington MS2 system. Bartington Instruments Ltd. *British Library London*.

Dekkers M.J. 1989. Magnetic properties of natural pyrrhotite. II. High-and low-temperature behaviour of Jrs and TRM as function of grain size. *Physics of the Earth and Planetary Interiors* 57: 266-283.

Dekkers M.J., Passier H.F. & Schoonen M.A.A. 2000. Magnetic properties of hydrothermally synthesized greigite (Fe3S4)—II. High- and low-temperature characteristics. *Geophysical Journal International* 141: 809-819.

Dunlop D.J. 1986. Coercive forces and coercivity spectra of submicron magnetites. *Earth and Planetary Science Letters* 78: 288-295.

Dunlop D.J. & Özdemir Ö. 1997. *Rock magnetism: fundamentals and frontiers*. Cambridge university press.

Eronen M. 1974. *The history of the Litorina Sea and associated holocene events.* University of Helsinki, Helsinki.

Evans M.E. & Heller F. 2003. *Environmental magnetism: principles and applications of enviromagnetics*. International Geophysics series, Academic press, Elsevier, California.

Glückert G., Rantala P. & Ristaniemi O. 1993. *Itämeren jääkauden jälkeinen rannansiirtyminen Pohjanmaalla*. Turun yliopiston maaperägeologian osaston julkaisuja, ISSN 0356-7400, Turun yliopisto, Turku.

Haavisto-Hyvärinen M. & Kutvonen H. 2007. Maaperäkartan käyttöopas. *Geological Survey of Finland, Espoo, Finland*.

Hunt C.P., Banerjee S.K., Han J.M., Solheid P.A., Oches E., Sun W.W. & Liu T.S. 1995. Rock-magnetic proxies of climate-change in the loess-paleosol sequences of the Western Loess Plateau of China. *Geophysical Journal International* 123: 232-244.

King J., Banerjee S.K., Marvin J. & Özdemir Ö. 1982. A comparison of different magnetic methods for determining the relative grain-size of magnetite in natural materials - some results from lake-sediments. *Earth and Planetary Science Letters* 59: 404-419.

Konert M. & Vandenberghe J.E.F. 1997. Comparison of laser grain size analysis with pipette and sieve analysis: a solution for the underestimation of the clay fraction. *Sedimentology* 44: 523-535.

Krs M., Novák F., Krsová M., Pruner P., Kouklíková L. & Jansa J. 1992. Magnetic properties and metastability of greigite-smythite mineralization in brown-coal basins of the Krušné hory Piedmont, Bohemia. *Physics of the Earth and Planetary Interiors* 70: 273-287.

Liu Q., Roberts A.P., Larrasoaña J.C., Banerjee S.K., Guyodo Y., Tauxe L. & Oldfield F. 2012. Environmental magnetism: principles and applications. *Reviews of Geophysics* 50.

Maher B.A. 1988. Magnetic properties of some synthetic sub-micron magnetites. *Geophysical Journal International* 94: 83-96.

Maher B.A. 2011. The magnetic properties of Quaternary aeolian dusts and sediments, and their palaeoclimatic significance. *Aeolian Research* 3: 87-144.

Muxworthy A.R., Turney J.N., Qi L., Baker E.B., Perkins J.R. & Abdulkarim M.A. 2023. Interpreting high-temperature magnetic susceptibility data of natural systems. *Frontiers in Earth Science* 11: 1171200.

Potter D.K. & Stephenson A. 1986. The detection of fine particles of magnetite using anhysteretic and rotational remanent magnetizations. *Geophysical Journal International* 87: 569-582.

Ramaswamy V. & Rao P.S. 2006. Grain size analysis of sediments from the northern Andaman Sea: comparison of laser diffraction and sieve-pipette techniques. *Journal of Coastal Research* 22: 1000-1009.

Reinholdsson M., Snowball I.F., Zillén L., Lenz C. & Conley D.J. 2013. Magnetic enhancement of Baltic Sea sapropels by greigite magnetofossils. *Earth and Planetary Science Letters* 366: 137-150.

Roberts A.P. 1995. Magnetic properties of sedimentary greigite (Fe3S4). *Earth and Planetary Science Letters* 134: 227-236.

Roberts A.P., Chang L., Rowan C.J., Horng C.-S. & Florindo F. 2011. Magnetic properties of sedimentary greigite (Fe3S4): An update. *Reviews of Geophysics* 49.

Skinner B.J., Erd R.C. & Grimaldi F.S. 1964. Greigite, the thio-spinel of iron; a new mineral. *American Mineralogist: Journal of Earth and Planetary Materials* 49: 543-555.

Snowball I.F. & Thompson R. 1988. The occurrence of Greigite in sediments from Loch Lomond. *Journal of Quaternary Science* 3: 121-125.

Snowball I.F. 1997. The detection of single-domain greigite (Fe3S4) using rotational remanent magnetization (RRM) and the effective gyro field (Bg): mineral magnetic and palaeomagnetic applications. *Geophysical Journal International* 130: 704-716.
Stephenson A. 1980. Gyromagnetism and the remanence acquired by a rotating rock in an alternating-field *Nature* 284: 48-49.
Stephenson A. & Snowball I.F. 2001. A large gyromagnetic effect in greigite. *Geophysical Journal International* 145: 570-575.
Stober J.C. & Thompson R. 1979. An investigation into the source of magnetic minerals in some Finnish lake sediments. *Earth and Planetary Science Letters* 45: 464-474.
Stroeven A.P., Hättestrand C., Kleman J., Heyman J., Fabel D., Fredin O., Goodfellow B.W., Harbor J.M., Jansen J.D. & Olsen L. 2016. Deglaciation of fennoscandia. *Quaternary Science Reviews* 147: 91-121.
Ucar H., Kletetschka G., Egli R., Mach K., Petronis M.S., Grison H., Scheidt S., Schnabl P. & Kdyr S. 2024. Enigmatic mixture of magnetite magnetofossils and diagenetic greigite as the magnetic carriers of the Early Miocene lacustrine sediments from the Most Basin in Central Europe. *Physics of the Earth and Planetary Interiors* 353: 107216.
Verwey E.J.W. 1939. Electronic conduction of magnetite (Fe3O4) and its transition point at low temperatures. *Nature* 144: 327-328.
Vuorela A., Lahdenperä A.-M., Penttinen T. & Posiva. 2009. *Review of Bothnian Sea shore-level displacement data and use of a GIS tool to estimate isostatic uplift*. Working report / Posiva, Posiva, Olkiluoto.